Available online at www.sciencedirect.com

ScienceDirect

Geochimica et Cosmochimica Acta 211 (2017) 307–321

Geochimica et Cosmochimica Acta

www.elsevier.com/locate/gca

Fe isotope fractionation during Fe(II) oxidation by the marine photoferrotroph *Rhodovulum iodosum* in the presence of Si – Implications for Precambrian iron formation deposition

Wenfang Wu [a,d], Elizabeth D. Swanner [b], Ilka C. Kleinhanns [c], Ronny Schoenberg [c], Yongxin Pan [d], Andreas Kappler [a,e,*]

[a] *Geomicrobiology, Center for Applied Geosciences, University of Tuebingen, Germany*
[b] *Department of Geological and Atmospheric Sciences, Iowa State University, Ames, IA, United States*
[c] *Isotope Geochemistry, Department of Geosciences, University of Tuebingen, Germany*
[d] *Key Laboratory of the Earth's Deep Interior, Institute of Geology and Geophysics, Chinese Academy of Sciences, Beijing, China*
[e] *Center for Geomicrobiology, Department of Bioscience, Aarhus University, Denmark*

Received 12 December 2016; accepted in revised form 24 May 2017; Available online 30 May 2017

Abstract

The iron (Fe) isotopic composition of Precambrian iron formations (IFs), besides providing geological context through its mineralogical properties, was suggested to function as a biosignature that can be used to infer a potential microbial role in the formation of the deposited Fe minerals. Anoxygenic phototrophic Fe(II)-oxidizing bacteria (photoferrotrophs), capable of oxidizing Fe(II) anoxically using light energy, were potentially involved in Fe(II) oxidation in anoxic or suboxic Precambrian oceans. The effect of Si on Fe isotopic fractionation between aqueous Fe(II) and Fe–Si-co-precipitates has been investigated before. However, it is currently unknown how stable Fe isotopes are fractionated during enzymatic Fe(II) oxidation under marine hydrogeochemical conditions, and particularly how the presence of Si affects the Fe isotope composition and the isotopic exchange among different Fe phases. We therefore studied Fe isotope fractionation during Fe(II) oxidation by the marine photoferrotroph *Rhodovulum iodosum* in simulated Precambrian seawater amended with 1 mM dissolved Si. Our results show that the change in the Fe isotope compositions over time for both the initial aqueous Fe(II) (Fe_{aq}) and the Fe(III) precipitates (Fe_{ppt}) follow a Rayleigh distillation model. Moreover, the fractionation ($\varepsilon^{56}Fe_{ppt\text{-}aq}$) determined independently from either $\delta^{56}Fe_{aq}$ or $\delta^{56}Fe_{ppt}$ data resulted in a value of 2.3 ± 0.3 (2SD, $N = 6$). This value differs from the fractionation factor determined previously for Fe(II) oxidation by *R. iodosum* in the absence of Si, where the fractionation calculated from $\delta^{56}Fe_{aq}$ (i.e. 0.96–1.18) was different from that calculated from $\delta^{56}Fe_{ppt}$ (1.96–1.98). This difference was attributed to isotopic exchange processes with soluble and sorbed Fe species. The present study suggests that Si present in Precambrian oceans retards Fe isotopic exchange, likely through combined effects of complexation of dissolved Fe species by Si and sorption of Si to Fe(III) minerals, thus lowering sorption of Fe(II) to the Fe(III) minerals, which is necessary for isotopic exchange. In summary our data suggests that Si in ancient oceans played a key role for the Fe isotope composition of Fe(III) minerals that were deposited by photoferrotrophic iron oxidation in Precambrian oceans by minimizing subsequent isotope exchange and recrystallization processes with aqueous Fe(II).

Keywords: Banded iron formations; Precambrian ocean; Phototrophic iron oxidation; Bacteria; Iron isotopes; Silica

* Corresponding author at: Geomicrobiology, Center for Applied Geosciences, University of Tuebingen, Sigwartstrasse 10, D-72076 Tuebingen, Germany. Fax: +49 7071 29 295059.
E-mail address: andreas.kappler@uni-tuebingen.de (A. Kappler).

http://dx.doi.org/10.1016/j.gca.2017.05.033
0016-7037/

1. INTRODUCTION

Iron- and silica-rich chemical sedimentary rocks that deposited directly from Precambrian oceans, such as Precambrian iron formations (IFs), mainly formed from the mid-Archean to the early Proterozoic, 3.5–1.8 billion years (Gy) ago. IFs are significant archives of information about ancient seawater chemistry as well as ambient marine redox conditions (Anbar and Knoll, 2002; Bekker et al., 2010). Though oxygenic photosynthesis is thought to have appeared long before the Great Oxidation Event (GOE) at ~2.33 Gy ago, the ocean and atmosphere on early Earth were still poor in oxygen before the first appearance of oxygenic photosynthesis (Holland, 2002; Crowe et al., 2013; Planavsky et al., 2014; Luo et al., 2016). Phototrophic Fe (II)-oxidizing bacteria that were capable of using light as an energy source (anoxygenic photosynthesis) (Ehrenreich and Widdel, 1994) were therefore suggested to be involved in Fe(II) oxidation under anoxic conditions, while microaerophilic Fe(II)-oxidizing bacteria may have been involved under suboxic conditions (Chan and Emerson, 2016), consequently contributing to biological Fe mineral deposition in Archean IF (Konhauser et al., 2002; Kappler et al., 2005; Hegler et al., 2008; Posth et al., 2008; Croal et al., 2009; Wu et al., 2014; Gauger et al., 2015).

Various geological textures and mineralogical properties are documented to function as potential biosignatures for the involvement of microbes in IF depositional processes. Distinct twisted organic stalks associated with Fe(III) minerals are produced during Fe(II) oxidation by microaerophilic Fe(II)-oxidizing bacteria (Chan et al., 2011), and the twisted morphology as well as the organic matrix are able to withstand diagenetic temperatures and pressures (Picard et al., 2015). Fossils of twisted stalks have indeed been found in the 1.7 Gy Jhamarkotra Formation (Crosby et al., 2014) and very recently have been suggested to be present even in the 3.77–4.28 Gy old ferruginous rocks from the Nuvvuaqittuq belt in Quebec, Canada (Dodd et al., 2017). Photoferrotrophs that grew with Fe (II) produced specific and distinct hopanoids (i.e. C-2 methylated pentacyclic triterpenoids) during enzymatic Fe (II) oxidation (Eickhoff et al., 2013). Indeed, signatures of such organic molecules were preserved in the 1.88 Gy Gunflint cherts despite diagenetic temperatures of 150–170 °C (Alleon et al., 2016). Possible microbially-derived organic molecular fossils (biomarkers) of photoferrotrophs have been detected in the Early Quaternary IF-like rocks (Fru et al., 2013). Yet none of these biosignatures have been detected in IFs that were deposited prior to the GOE, when photoferrotrophs (and maybe to some extent also microaerophiles) likely participated in Fe(II) oxidation in the Archean column water. Thus, there is a need to establish robust biosignatures for Fe(II)-oxidizing microbes in Fe-rich rocks, and Fe isotope signatures retained in IFs are a target.

While geological structures and mineralogical properties provided some insights into the bacterial roles in mineral deposition, isotope compositions in IFs also record possible biological processes in ancient oceans and/or within the resulting sediments (Johnson et al., 2003; Johnson et al., 2008b; Czaja et al., 2010; Heimann et al., 2010). The redox transformation between Fe(II) and Fe(III), both abiotic and biologically mediated, causes Fe isotope fractionation at ambient temperature (Crosby et al., 2005; Johnson et al., 2005; Balci et al., 2006; Wu et al., 2009; Kappler et al., 2010; Percak-Dennett et al., 2011; Swanner et al., 2015). Such fractionation in Fe isotopes could be preserved in the Fe minerals in IFs that deposited from Precambrian oceans (Beard et al., 1999; Johnson et al., 2008a; Planavsky et al., 2012; Czaja et al., 2013; Hashizume et al., 2016). During redox transformation, the Fe(III) tends to become enriched in heavy isotopes, leading to a residual Fe(II) pool that is consequently enriched in the light Fe isotopes (Anbar et al., 2000; Skulan et al., 2002; Johnson et al., 2008b). For instance, Fe isotope values recorded in Precambrian sedimentary pyrites were sensitive to the concentration of dissolved Fe(II) in ancient ocean and extent of Fe(II) oxidation, where variable and negative Fe isotopes dominate in pyrites formed before 2.3 Gy (Rouxel et al., 2005), suggesting the capability of Fe isotope in recording Fe redox processes.

Various studies documented a consistent equilibrium δ^{56}Fe isotope fractionation of around −3‰ between aqueous Fe(II) [$Fe(II)_{aq}$] and aqueous Fe(III) [$Fe(III)_{aq}$] (Skulan et al., 2002; Welch et al., 2003) in abiotic systems. Microbially catalyzed Fe redox processes also generate a significant Fe isotope fractionation (Beard et al., 1999, 2003a; Johnson and Beard, 2005). Enzymatic Fe(II) oxidation by acidophilic and nitrate-reducing Fe(II)-oxidizing bacteria resulted in δ^{56}Fe isotope fractionation of around −3‰ as well (Balci et al., 2006; Kappler et al., 2010). For modern photoferrotrophs, an δ^{56}Fe isotopic fractionation of −1.5 ± 0.2‰ between $Fe(II)_{aq}$ and $Fe(III)_{ppt}$ was determined using the freshwater strain *Thiodictyon F4* (Croal et al., 2004). Yet this may not represent Archean oceans bearing a significant concentration of chloride, which is able to affect the reactivity of Fe species and consequently the Fe isotopic exchange (i.e. 0.3‰ decrease in the fractionation factor per mol Cl^- on average) (Hill et al., 2010). Indeed, a study using the marine photoferrotroph *Rhodovulum iodosum* reported δ^{56}Fe isotope fractionations between $Fe(II)_{aq}$ and $Fe(III)_{ppt}$ ranging from −0.96‰ to −1.98‰ (Swanner et al., 2015), i.e. significantly larger and more variable than the Fe isotope fractionation observed by Croal et al. (2004) for the freshwater strain F4.

Although some data on Fe isotope fractionation during microbial Fe(II) oxidation exists, there is little constraint regarding Fe isotope fractionation during biological Fe (II) oxidation under Si-rich conditions of Archean oceans (Maliva et al., 2005). Geological investigation of Precambrian IFs and shales suggested that, in the Si-rich Precambrian oceans that contained up to 2.2 mM Si (Maliva et al., 2005), dissolved Fe was likely precipitated as primary Fe-silicates instead of iron (oxyhydr)oxides (Rasmussen et al., 2013, 2015). Moreover, an authigenic greenalite mineral was synthesized experimentally with Fe^{2+} and SiO_2(aq) in anoxic seawater (Tosca et al., 2016). Recent Si isotope fractionation investigations in both biotic and abiotic experiments indicate strong isotope exchange of aqueous Si with Fe-silicate and Fe–Si gel (Reddy et al., 2016; Zheng et al., 2016). Si is capable of affecting Fe speciation

by complexation, adsorption, polymerization, and co-precipitation (Doelsch et al., 2000, 2001, 2003; Jones et al., 2009), which affects Fe isotopic exchange and thus the overall Fe isotope fractionation during Fe redox transformations (Wu et al., 2009, 2012; Percak-Dennett et al., 2011). Therefore, Fe isotope fractionation during phototrophic Fe(II) oxidation in the presence of Si is a relevant process to consider in the generation of potential Fe isotope biosignatures in IFs deposited from Precambrian oceans, as they were saturated with respect to amorphous silica and/or cristobalite (Si 0.67–2.2 mM) (Maliva et al., 2005).

Based on this knowledge gap the aim of this study was to experimentally determine Fe isotope fractionation during enzymatic Fe(II) oxidation by a marine photoferrotroph under simulated Archean anoxic ferruginous ocean conditions, considering in particular the high Si content. The marine strain *R. iodosum* was cultivated phototrophically in the presence of 1 mM dissolved Si with Fe(II) as the sole electron donor. The different Fe species such as $Fe(II)_{aq}$, $Fe(III)_{ppt}$, and intermediate Fe species (i.e. adsorbed, colloidal, and organically complexed Fe) present during microbial Fe(II) oxidation were separated by sequential extractions. The Fe concentration and Fe isotope composition of all separated fractions was quantified in order to determine the Fe isotope fractionation during Fe(II) oxidation and the effect of Si on isotopic exchange during enzymatic Fe(II) oxidation and during Fe mineral deposition in Precambrian IF.

2. MATERIALS AND METHODS

2.1. Bacterial strain and culture medium

The marine photoferrotroph *Rhodovulum iodosum* was isolated from a mud flat of the North Sea (Straub et al., 1999). Marine phototroph (MP) medium (pH 6.8, 22 mM bicarbonate buffer) was prepared anoxically in a Widdel flask as described by Swanner et al. (2015). Fe(II) was added to the MP medium from a 1 M $FeCl_2$ stock solution. Si was supplemented from a 50 mM $Na_2SiO_3{\cdot}9H_2O$ stock solution at a final concentration of 1 mM, i.e. within the concentration range estimated for the Archean ocean (Maliva et al., 2005). After these additions, the medium was filtered (0.22 μm) in an anoxic glovebox (100% N_2) to remove Fe precipitates such as vivianite and siderite (Hohmann et al., 2009), which is necessary to allow the exact determination of the isotopic composition of subsequently formed Fe(III) minerals. Additions of trace elements, vitamins, and a selenium and tungstate solution (that were required by the microorganisms for growth) were added after filtration to avoid loss by sorption to minerals. The headspace of the medium was flushed with N_2/CO_2 (v/v, 90/10) before use to keep an anoxic atmosphere in the culturing bottles thus simulating Archean seawater conditions and providing suitable conditions for growth of *R. iodosum* (Wu et al., 2014; Swanner et al., 2015).

To prepare the microbial inoculum, *R. iodosum* cells were grown to late-exponential phase in MP medium with H_2 instead of Fe(II) as electron donor (headspace flushed with H_2/CO_2, v/v, 80/20) to avoid any Fe minerals in the new medium stemming from the inoculum. Cells were inoculated into the Si-containing Fe(II) medium (final concentration $2.7 * 10^7$ cells mL^{-1}), and cultured in closed serum bottles (50 mL medium in 120 mL serum bottle) at 26 °C under light intensity of 600 lux (12 μmol quanta m^{-2} s^{-1}). Experiments were conducted with three independent biological replicates (named Ri-1, Ri-2 and Ri-3).

2.2. Sequential extraction of different Fe species and Fe analysis

During incubation, samples were taken from the three serum bottles using sterile syringes in the anoxic glovebox. Several Fe species were present, i.e. Fe(II) or Fe(III) in aqueous solution (Fe_{aq}), Fe(II) or Fe(III) precipitates/minerals (Fe_{ppt}), and intermediate phases (collectively called Fe_{interm}) such as Fe(II) or Fe(III) adsorbed to the cells or Fe minerals, colloids, etc. To separate different Fe species, sequential extraction was conducted by washing, centrifugation and filtration as described before (Swanner et al., 2015). Specifically, 1 mL of culture slurry was centrifuged at 13,000*g* for 10 min. The supernatant was filtered through a 0.22 μm centrifuge tube filter (Costar spin-X, Corning, USA) to collect the aqueous fraction (Fe_{aq}). The pellet (solids at the bottom of the tube after centrifugation) went through a two-step washing, first with anoxic high purity H_2O (MilliQ, 18.2 MΩ cm^{-1}), and second with an anoxic sodium acetate solution (0.5 M NaAc, pH adjusted to 4.85 with acetic acid). The supernatants after H_2O and NaAc washing (termed Fe_{H2O} and Fe_{NaAc}) were collected individually, and stored in 1 M HCl for further Fe concentration and Fe isotope analysis. The final Fe precipitates (Fe_{ppt}) after the two-step washing were dissolved in 6 M HCl. All sampling, washing, centrifuging and filtration steps for sequential extraction were conducted in an anoxic glovebox (100% N_2).

After separation, both Fe(II) and total Fe concentrations were quantified in the different fractions (Fe_{aq}, Fe_{H2O}, Fe_{NaAc} and Fe_{ppt}) by the ferrozine assay (Stookey, 1970). The initial Fe(II) concentration for the medium after filtration was 1.2 mM. Si concentration of the medium after filtration was 1.0 mM determined in a microtiterplate photospectrometer (Multiskan Go, Thermo Scientific) using the molybdenum blue method (Strickland and Parsons, 1972). Micro X-ray diffraction (Bruker D8 Discover XRD, Bruker, Germany) was conducted on the final products in order to identify the mineralogy of the precipitates.

2.3. Fe isotope analysis

Fe purification and isotope analysis were conducted for the collected Fe fractions ($\delta^{56}Fe_{aq}$, $\delta^{56}Fe_{ppt}$, $\delta^{56}Fe_{H2O}$ and $\delta^{56}Fe_{NaAc}$) at the facilities of the Isotope Geochemistry group of the University of Tübingen. All samples were first amended with an adequate amount of a ^{57}Fe–^{58}Fe-enriched tracer solution, which allows correction of any mass-dependent isotope fractionation induced during chemical purification and mass spectrometric isotope measurement (Schoenberg and von Blanckenburg, 2005). All acids used for digestion, purification, and later as matrix for isotope

measurements were distilled from p.a. grade acids using Savillex© DST 1000 stills. For purification, sample aliquots between 2 and 5 μg Fe went through Spectrum® 104704 polypropylene columns that were embedded with 1 mL of anion exchange resin (Dowex AG-1x8 100–200 mesh) following the procedure described in Schoenberg and von Blanckenburg (2005). A procedural blank was run together with processed samples, which indicated a less than 0.25% impurity contribution of Fe to the least concentrated samples, and is thus negligible.

After purification, samples were re-suspended in 1.5 mL of 0.3 M HNO_3 and the Fe isotope compositions were measured on a ThermoFisher Scientific NeptunePlus multi-collector inductively coupled plasma mass spectrometer. All four Fe ion beams, together with $^{52}Cr^{+}$ and $^{60}Ni^{+}$ as interference monitors for ^{54}Cr on ^{54}Fe and ^{58}Ni on ^{58}Fe, respectively, were detected simultaneously for 90 cycles each with 8 s integration time. Polyatomic interferences such as ArN and ArO were avoided by measuring in high-resolution mode. Background corrections were made based on on-peak-zero measurements of the pure analyte solution prior and after each sample analysis. Data are reported relative to the isotopically certified international reference material IRMM-014 using the δ-notation (Eq. (1)), reported in ‰.

$$\delta^{56}Fe = \left(\frac{^{56}Fe/^{54}Fe_{sample}}{^{56}Fe/^{54}Fe_{IRMM\text{-}014}} - 1\right) \times 1000 \quad (1)$$

The reproducibility in $\delta^{56}Fe$ of the HanFe in-house standard during the course of this study was 0.288 ± 0.037‰ (2SD, $N = 10$), equivalent to the long-term reproducibility of $\delta^{56}Fe = 0.287 \pm 0.055$‰ (2SD, $N = 145$). These values agree well with the $\delta^{56}Fe$ value of 0.290 ± 0.070 for this standard solution reported in a previous study (Moeller et al., 2014). The TübFe standard yielded $\delta^{56}Fe$ of −0.371 ± 0.084‰ (2SD, $N = 5$). The reproducibility for IRMM-014 was 0.000 ± 0.055‰ (2SD, $N = 20$), which defined the minimum 2σ uncertainty of measurements. The in-run precision of individual samples is reported when this value is larger than 0.055‰. The $\delta^{56}Fe_{aq}$ and $\delta^{56}Fe_{ppt}$ at different fractions of residual Fe(II) (f) were fit with Rayleigh equations (Eqs. (2) and (3)) for closed system in order to obtain the fractionation factor α (Eq. (4)), which can be transformed to the isotopic fractionation $\varepsilon^{56}Fe$ (Eq. (5)).

$$\delta^{56}Fe_{aq} = [\delta^{56}Fe_{aq}(t = 0) + 1000] \times f^{\alpha-1} - 1000 \quad (2)$$

$$\delta^{56}Fe_{ppt} = [\delta^{56}Fe_{aq}(t = 0) + 1000] \times (1 - f^{\alpha})/(1 - f) - 1000 \quad (3)$$

$$\alpha_{A-B} = \frac{\delta^{56}Fe_A}{\delta^{56}Fe_B} \quad (4)$$

$$\varepsilon_{A-B} = 10^3 \ln \alpha_{A-B} \approx (\alpha_{A-B} - 1) \times 1000 \quad (5)$$

3. RESULTS

3.1. Fe(II) oxidation rates and Fe concentrations of different Fe fractions (Fe_{aq}, Fe_{H2O}, Fe_{NaAc} and Fe_{ppt})

In order to determine phototrophic Fe(II) oxidation rates by *R. iodosum* in the presence of Si and the change of different Fe species over time, the concentrations of all collected Fe fractions were quantified (see Table 1) and data for a representative setup (Ri-3) is plotted in Fig. 1. The fastest Fe(II) oxidation rates were measured 72 h after inoculation, while before that Fe(II) oxidation was slower (Fig. 1). Within the first 72 h, ca. 34% of Fe(II) was removed from solution, without visible formation of Fe (III) particles, which is similar to a previous study of Fe (II) oxidation by *R. iodosum*, suggesting a prolonged lag phase for cell growth in the presence of Si (Wu et al., 2014). An average Fe(II) oxidation rate of 29 ± 2 μM/h was measured after 72 h incubation in the presence of Si (1 mM). It was faster than that observed in experiments without Si addition at 1.26 mM initial Fe(II) (0.37 mM/day or 15 μM/h) (Wu et al., 2014), but similar to the value observed for green sulfur phototrophic Fe(II)-oxidizing bacteria, where the presence of Si enhanced Fe(II) oxidation rates (Gauger et al., 2016). The $Fe(II)_{aq}$ was completely oxidized by *R. iodosum* over the 96-h incubation period (Fig. 1a), leading to the accumulation of orange Fe(III) minerals at the bottom of the bottles. The micro-XRD pattern of the final Fe(III) precipitates did not show any visible diffraction signals (Fig. 2), indicating the mineral product to be X-ray amorphous or short range ordered, such as the case for ferrihydrite (Wu et al., 2014).

During phototrophic Fe(II) oxidation, the Fe speciation of the different Fe fractions changed over time. In the aqueous Fe fraction (Fe_{aq}) that was separated by centrifugation followed by filtration, no $Fe(III)_{aq}$ was present for most of the samples except the 90-h sample, where 234 μM Fe(III) was detected, likely representing smaller than 0.22 μm colloidal Fe(III) that passed the filter (Fig. 1a). The presence of colloidal Fe(III) only in the middle stage of phototrophic Fe(II) oxidation might be due to Fe(III) accumulation by rapid Fe(II) oxidation, leading to the formation of colloidal Fe(III) species. In the Fe precipitate fraction (Fe_{ppt}), after a two-step washing procedure, the remaining Fe(II) detected was less than 8 μM corresponding to maximally 1% of the Fe precipitates (Fig. 1b), which was negligible for further isotope fractionation factor determination by Rayleigh fitting. In the Fe_{H2O} and $Fe_{NaAc,}$ fractions, the Fe was present as a mixture of Fe(II) and Fe(III). Over time, Fe(III) in Fe_{H2O} and Fe_{NaAc} increased, while Fe(II) first increased to up to 67 μM (or 5% relative to the total Fe) and then dropped quickly to values below 22 μM (or 1.6% relative to the total Fe pool). More Fe was present in the Fe_{NaAc} fraction compared to Fe_{H2O}, where the maximum Fe(II) and Fe(III) concentrations reached 67 μM and 164 μM in the Fe_{NaAc} fraction, respectively, and 8 μM and 53 μM of Fe(II) and Fe(III), respectively, in the Fe_{H2O} fraction.

3.2. Fe isotope compositions of Fe_{aq}, Fe_{H2O}, Fe_{NaAc} and Fe_{ppt}

The Fe isotope compositions of all four sequentially separated fractions (Fe_{aq}, Fe_{H2O} Fe_{NaAc}, and Fe_{ppt}) from the three independent biological replicates (Ri-1, Ri-2 and Ri-3) were analyzed and are reported in Table 2. The initial substrate Fe(II) had a $\delta^{56}Fe$ value of on average −0.379 ± 0.019‰ (2SD; $n = 3$). In parallel to the gradual Fe(II) oxidation, the $\delta^{56}Fe$ values decreased over time for both Fe_{aq}

Table 1
Fe(II) and Fe(total) concentrations for each of the fractions separated in each experimental replicate. Fe quantifications were made using the spectrophotometric Ferrozine assay. One standard deviation (SD) of triplicated measurements (analytical error) is reported. Fe(III) was calculated as the difference between Fe(total) and Fe(II).

Time (h)	Frac. $Fe(II)_{ox}$	Fe Frac.	Fe(II) (μM)	1SD	Fe(tot) (μM)	1SD	Fe(III) (μM)	Recovery (%)
Experiment replicate Ri-1								
0	0	aq	1362.9	5.5	1360.9	31.8	BD	100.2
		ppt	ND		ND		ND	
		H_2O	ND		ND		ND	
		NaAc	ND		ND		ND	
72	0.35	aq	889.8	3.3	877.7	2.0	BD	94.2
		ppt	5.2	0.3	306.5	2.1	301.3	
		H_2O	0.9	0.2	9.6	0.3	8.8	
		NaAc	55.1	1.2	87.5	0.6	32.3	
80	0.61	aq	526.5	3.5	513.7	6.5	BD	100.1
		ppt	7.5	3.2	641.8	3.0	634.3	
		H_2O	3.8	0.1	56.4	0.6	31.8	
		NaAc	65.1	0.6	149.8	3.3	84.7	
90	0.75	aq	339.6	2.3	573.9	3.9	234.3	
		ppt	7.4	0.7	1140.7	6.9	1133.3	
		H_2O	2.6	0.5	35.7	1.1	53.8	
		NaAc	52.2	0.3	137.9	2.2	85.8	
96	1.00	aq	BD		BD		BD	98.3
		ppt	4.4	2.6	1104.8	9.2	1100.5	
		H_2O	0.1	0.5	47.2	0.5	47.1	
		NaAc	20.9	0.6	185.3	0.9	164.5	
Experiment replicate Ri-2								
0	0.00	aq	1336.8	3.8	1312.5	1.7	BD	101.9
		ppt	ND		ND		ND	
		H_2O	ND		ND		ND	
		NaAc	ND		ND		ND	
72	0.26	aq	989.8	15.2	961.5	2.2	BD	107.6
		ppt	20.9	1.3	334.8	2.2	313.9	
		H_2O	6.3	0.5	22.8	0.7	16.5	
		NaAc	56.9	1.7	92.6	1.2	35.7	
80	0.43	aq	756.6	12.3	729.2	174.5	BD	100.3
		ppt	5.8	2.5	454.5	3.5	448.6	
		H_2O	3.0	0.1	26.5	0.8	23.5	
		NaAc	67.0	0.4	106.6	2.6	39.6	
90	0.52	aq	648.1	4.4	745.6	23.3	97.5	133.3
		ppt	8.6	2.3	849.9	12.5	841.3	
		H_2O	3.8	0.3	48.4	1.1	44.6	
		NaAc	63.0	1.3	105.6	13.3	42.7	
96	0.87	aq	171.5	5.6	161.1	0.6	BD	133.6
		ppt	6.1	1.1	1383.3	3.4	1377.2	
		H_2O	1.2	0.2	51.5	0.9	50.4	
		NaAc	46.0	0.2	157.9	1.2	111.9	
Experiment replicate Ri-3								
0	0.00	aq	1335.3	5.6	1345.7	37.1	10.4	99.2
		ppt	ND		ND		ND	
		H_2O	ND		ND		ND	
		NaAc	ND		ND		ND	
72	0.34	aq	879.7	8.3	867.4	8.3	BD	88.0
		ppt	3.6	3.2	201.3	1.7	197.7	
		H_2O	7.9	0.2	25.6	0.6	17.7	
		NaAc	61.0	0.9	90.3	0.4	29.2	

(*continued on next page*)

Table 1 (*continued*)

Time (h)	Frac. $Fe(II)_{ox}$	Fe Frac.	Fe(II) (μM)	1SD	Fe(tot) (μM)	1SD	Fe(III) (μM)	Recovery (%)
80	0.55	aq	604.0	7.2	607.6	5.7	3.6	108.9
		ppt	8.0	1.6	710.9	12.6	702.9	
		H_2O	1.6	0.4	27.3	0.3	25.6	
		NaAc	62.0	0.4	119.2	1.9	57.2	
90	0.66	aq	449.5	5.2	693.9	7.8	244.4	130.3
		ppt	7.9	1.6	892.4	2.5	884.5	
		H_2O	2.9	0.2	45.0	0.8	42.1	
		NaAc	54.3	0.4	121.5	1.0	67.2	
96	1.00	aq	BD		BD		BD	105.7
		ppt	4.5	1.1	1199.1	10.8	1194.6	
		H_2O	BD		50.2	0.6	50.2	
		NaAc	21.83	1.04	172.88	2.40	151.05	

BD = Iron concentrations were below the detection limit of our method (0.01 mM). ND = Iron concentration was not determined for this fraction.

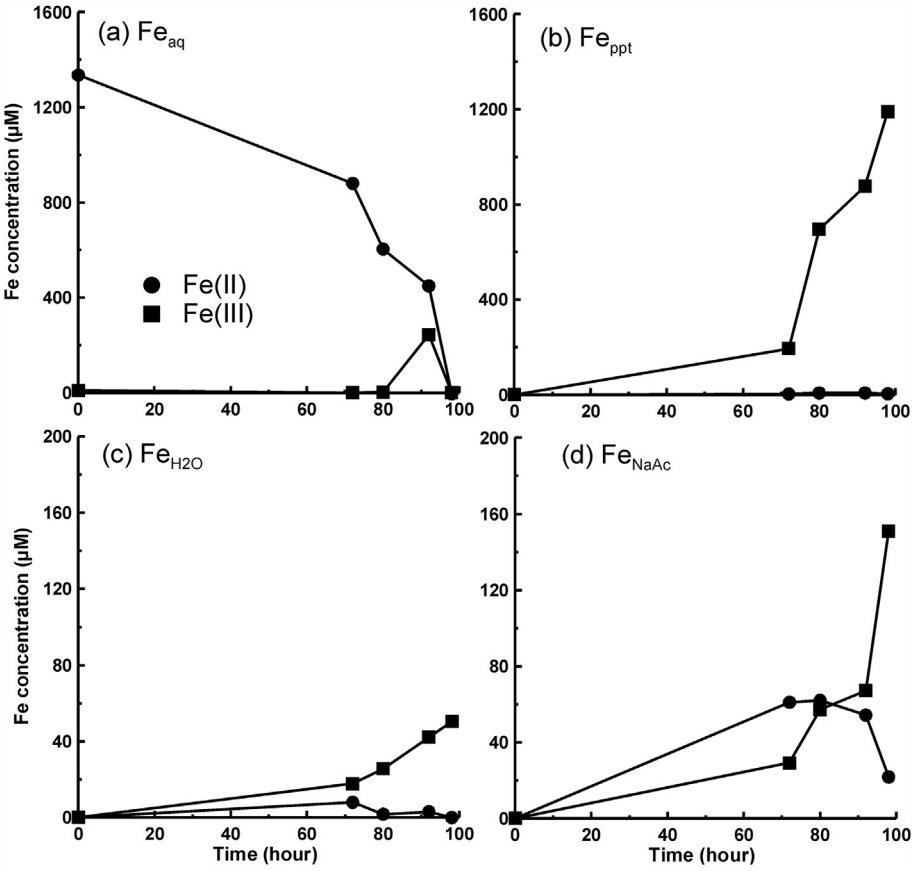

Fig. 1. Concentrations of Fe(II) (in circles) and Fe(III) (in squares) species over time during a representative incubation (Ri-3) of *R. iodosum*. The different Fe species were separated by sequential extraction. (a) Aqueous Fe (Fe_{aq}), (b) Fe precipitates (Fe_{ppt}), (c) H_2O-extracted fraction (Fe_{H2O}), and (d) NaAc-extracted fraction (Fe_{NaAc}). Error bars (smaller than symbol size in all cases) show the standard deviation of triplicate analyses.

and Fe_{ppt} (Fig. 3), while the remaining Fe_{aq} (mainly $Fe(II)_{aq}$) showed preferential enrichment in lighter Fe isotopes compared to the Fe_{ppt} (mainly $Fe(III)_{ppt}$). When all Fe(II) was oxidized, the Fe_{ppt} reached the initial $\delta^{56}Fe$ value of the initial $Fe(II)_{aq}$ (Fig. 3). The experimentally obtained maximum $\delta^{56}Fe_{ppt}$ after 34% Fe(II) oxidation was 1.662‰ (Ri-3), and the minimum $\delta^{56}Fe_{aq}$ after 87% Fe(II) oxidation was −4.122‰ (Ri-2). These extreme values for $Fe(II)_{aq}$ and $Fe(III)_{ppt}$ illustrate limitations in sampling and isotope measurements for our Fe(II) oxidation experiments.

The isotope compositions for the Fe_{H2O} and Fe_{NaAc} fractions which contained both Fe(II) and Fe(III)

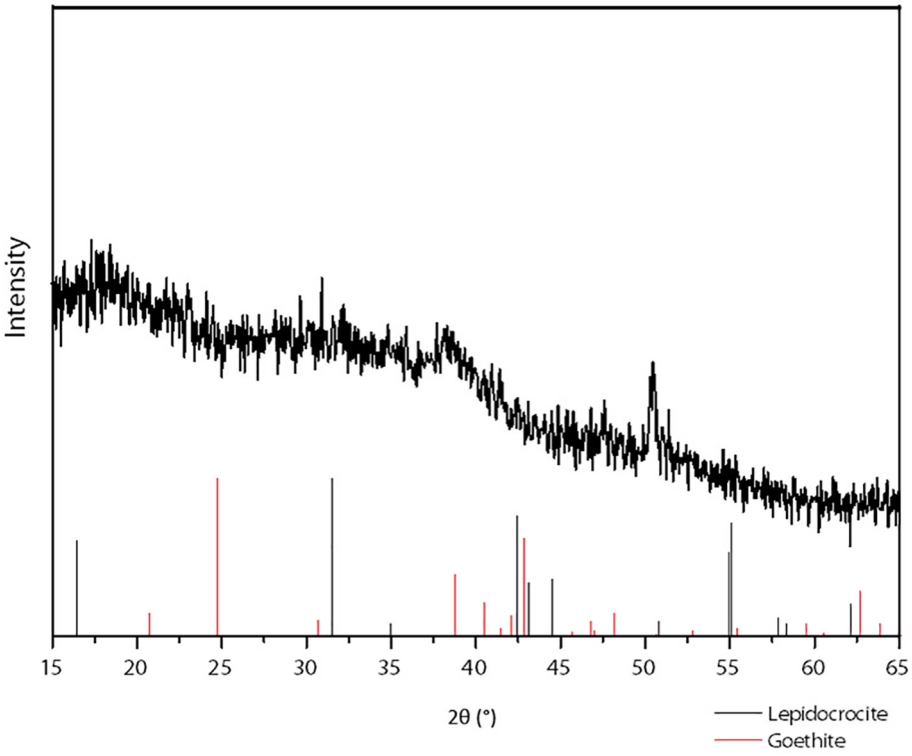

Fig. 2. X-ray diffractogram for the final Fe(III) precipitates after all Fe(II) (1.2 mM) was oxidized to Fe(III) by *R. iodosum* in the presence of 1 mM Si.

resembled neither Fe_{aq} nor Fe_{ppt}. Instead, their $\delta^{56}Fe$ values were in between the corresponding Fe_{aq} and Fe_{ppt} fractions and showed a slightly decreasing trend over time. The $\delta^{56}Fe_{H2O}$ was slightly heavier than $\delta^{56}Fe_{NaAc}$, i.e. Fe_{H2O} had always slightly positive $\delta^{56}Fe$ values, while Fe_{NaAc} had slightly negative $\delta^{56}Fe$ values with only a few exceptions.

4. DISCUSSION

4.1. Changes in Fe speciation during the progress of microbial Fe(II) oxidation

Phototrophic Fe(II) oxidation by *Rhodovulum iodosum* was recently investigated in the absence of Si (Swanner et al., 2015), in which the same sequential extraction procedures were applied to separate and analyze the different Fe species. A careful comparison to the previous study allows us to determine possible effects of Si in changing the Fe speciation during phototrophic Fe(II) oxidation.

Intermediate Fe(II) phases (likely adsorbed and colloidal Fe) formed as phototrophic Fe(II) oxidation proceeded, which were collected in Fe_{H2O} and Fe_{NaAc} fractions. Fe(II) initially increased in both Fe_{H2O} and Fe_{NaAc} fractions, then decreased as Fe(II) oxidation proceeded (Fig. 1). A similar trend was observed in experiments without Si (Swanner et al., 2015). However, in the presence of Si, much less Fe(II) (8 μM, or 0.7% relative to the total Fe pool) was present in the Fe_{H2O} fraction compared to that without Si (around 100 μM, representing 2.5%). This is at least partially attributable to the lower concentration of the initial $Fe(II)_{aq}$, as the amount of Fe (II) extracted by sodium acetate was again much less than that without Si (60 μM vs. 150 μM, representing 5% vs. 3.75%, respectively), but comparable in percentage relative to the initial Fe(II) substrate concentration. However, this lower amount of Fe(II) to some extent, suggests an effect of the Si on Fe(II) extractability. Si can adsorb on synthesized ferrihydrite at room temperature, which contributes to Si isotope exchange (Delstanche et al., 2009). Moreover, competition of Si with Fe(II) for adsorption sites at the surface of Fe(III) minerals was reported (Jones et al., 2009). This would result in less sorbed Fe(II) on Fe precipitates in our experimental system with dissolved Si. A recent Si isotope study with aqueous Si and an Fe(III)-Si gel even suggested the formation Si–O–Fe bonds (Zheng et al., 2016), which in turn suggested the potential of Si in changing Fe speciation and thus influencing Fe isotope fractionation.

The concentrations of the intermediate Fe(III) phases (adsorbed, complexed, or poorly crystalline colloidal Fe (III)) in the Fe_{H2O} and Fe_{NaAc} fractions increased over time, and the maximum concentrations were higher than $Fe(II)_{interm}$. In the presence of Si, Fe(III) concentrations in the Fe_{H2O} or Fe_{NaAc} fractions were around 50 μM (4%) for Fe_{H2O}, and 170 μM (14%) for Fe_{NaAc}, respectively, values comparable to the experiments without Si, which was also conducted using the same medium (pH 6.8) and

Table 2
Fe isotope composition of different Fe species (Fe_{aq}, Fe_{ppt}, Fe_{H2O} and Fe_{NaAc}) measured during Fe(II) oxidation by *R. iodosum* in triplicate experimental setups Ri-1, Ri-2, and Ri-3. External reproducibility of 0.055‰ is derived from replicate measurement of the IRMM-014 standard (2SD). Bold values represent lower in-run precision from single sample measurement (2SE).

Fe species	Ri-1			Ri-2			Ri-3		
	Frac. $Fe(II)_{ox}$	$\delta^{56/54}Fe$ [‰]	2SE[a] [‰]	Frac. $Fe(II)_{ox}$	$\delta^{56/54}Fe$ [‰]	2SE[a] [‰]	Frac. $Fe(II)_{ox}$	$\delta^{56/54}Fe$ [‰]	2SE[a] [‰]
Fe_{aq}	0	−0.38	0.055	0	−0.37	0.055	0	−0.389	0.055
	0.35	−1.319	0.055	0.26	−1.042	0.055	0.34	−1.233	0.055
	0.61	−2.374	0.055	0.43	−1.727	0.055	0.55	−2.198	0.055
	0.75	−3.552	0.055	0.52	−2.312	0.055	0.66	−3.161	0.055
	1	ND[d]	ND	0.87	−4.122	0.055	1	ND	ND
Fe_{ppt}	0.35	1.66	0.055	0.26	1.521	0.055	0.34	1.662	0.055
	0.61	1.153	0.055	0.43	0.131	**0.091**	0.55	1.462	**0.088**
	0.75	0.611	0.055	0.52	1.19	0.055	0.66	0.749	0.055
	1	−0.191	0.055	0.87	0.384	0.055	1	−0.228	0.055
Fe_{H2O}	0.35	1.345	**0.115**[b]	0.26	ND	ND	0.34	0.758	**0.115**
	0.61	0.744	**0.056**	0.43	1.05	0.055	0.55	0.975	0.055
	0.75	0.42	0.055	0.52	0.856	0.055	0.66	0.567	0.055
	1	−0.667	0.055	0.87	0.196	0.055	1	−0.761	0.055
Fe_{NaAc}	0.35	−0.002	0.055	0.26	0.322	0.055	0.34	0.018	0.055
	0.61	−0.234	0.055	0.43	0.514	0.055	0.55	−0.154	0.055
	0.75	−0.527	0.055	0.52	−0.262	0.055	0.66	−0.449	0.055
	1	−1.481	**0.074**	0.87	−0.629	0.055	1	−1.668	0.055
$Fe(II)_{interm}$[c]	0.35	−0.925		0.26	−2.397		0.34	−0.632	
	0.61	−1.921		0.43	0.125		0.55	−1.332	
	0.75	−2.301		0.52	−1.136		0.66	−1.92	
	1	−8.045		0.87	−2.802		1	−7.795	
$Fe(III)_{interm}$[c]	0.35	1.571		0.26	4.656		0.34	1.376	
	0.61	1.063		0.43	1.17		0.55	1.123	
	0.75	0.552		0.52	1.027		0.66	0.74	
	1	−0.648		0.87	0.265		1	−0.782	

[a] Data taken from measurement of IRMM-014 (0.055 2SD, $N = 20$), for which the measured uncertainty is less than 0.055.
[b] Highlighted when uncertainties are larger than 0.055.
[c] Data were calculated according to assumptions and the mass balance described in text.
[d] ND = Not determined.

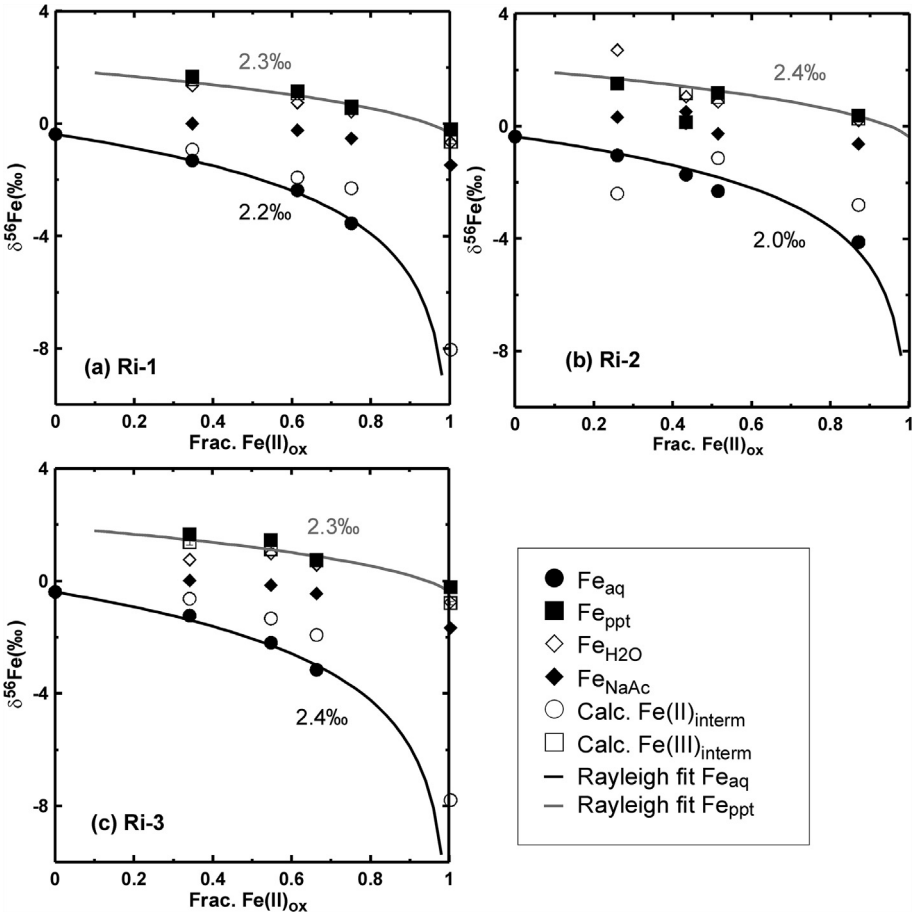

Fig. 3. Fe isotope composition of different Fe species (Fe_{aq}, Fe_{H2O}, Fe_{NaAc} and Fe_{ppt}) vs. extent of Fe(II) oxidation (Frac. $Fe(II)_{ox}$) for the three independent biological replicates, (a) Ri-1, (b) Ri-2 and (c) Ri-3. Lines showed the Rayleigh fitting of Fe_{aq} and Fe_{ppt} data with fitting $\varepsilon^{56}Fe_{ppt\text{-}aq}$ values shown in ‰. Calculated $Fe(II)_{interm}$ and $Fe(III)_{interm}$ (based on mass balance) were also plotted.

extraction procedures (Swanner et al., 2015). However, with regard to the percentage of Fe(III) in Fe_{H2O} and Fe_{NaAc} fractions relative to initial Fe(II) concentrations, more Fe (III) stayed in Fe_{H2O} and Fe_{NaAc} fractions in the presence of Si compared to that without Si (4% vs. 1% for Fe_{H2O}, and 14% vs. 4% for Fe_{NaAc}) (Swanner et al., 2015). Si was suggested to be able to prevent or at least slow down the transformation of Fe(III) to more stable, crystalline Fe (III) phases (Doelsch et al., 2000; Jones et al., 2009). In our experiments, the presence of Si likely stabilized the intermediate Fe(III) species (loosely adsorbed, colloidal, or associated with cells) in fractions of Fe_{H2O} and Fe_{NaAc} before they precipitated, probably by forming small Fe–Si aggregates (Doelsch et al., 2003; Jones et al., 2009).

In contrast to the Fe_{H2O} and Fe_{NaAc} fractions that contained both Fe(III) and Fe(II), the Fe_{aq} contained mainly Fe(II) (Table 1). This suggests that once aqueous Fe(III) was formed during phototrophic Fe(II) oxidation, these ions rapidly polymerized and associated with Si before they precipitated as Fe(III) minerals (Posth et al., 2014), leading to negligible aqueous Fe(III), in contrast to the experiments without Si in which maximum aqueous Fe(III) was 2.2% of the total aqueous Fe (Swanner et al., 2015). For the Fe_{ppt} fraction, only Fe(III) was detected, which suggests that no Fe(II) precipitates formed, similar to the experiments in the absence of Si (Swanner et al., 2015).

4.2. Fe isotope fractionation between $Fe(II)_{aq}$ and $Fe(III)_{ppt}$ during phototrophic Fe(II) oxidation

The formation of Fe(III) (oxyhydr)oxides by phototrophic Fe(II)-oxidizing bacteria involves enzymatic oxidation of $Fe(II)_{aq}$ to $Fe(III)_{aq}$, and the polymerization of $Fe(III)_{aq}$ to form colloidal phases, which ultimately precipitate as $Fe(III)_{ppt}$. Additionally, processes such as Fe(II)/Fe (III) adsorption to Fe_{ppt} (Icopini et al., 2004; Crosby et al., 2007), complexation of $Fe(III)_{aq}$ by cell-derived biomolecules (Swanner et al., 2015), and/or Fe(II)-catalyzed Fe-isotope and electron exchange processes (Handler et al., 2009) may also take place, all of which impose Fe isotope fractionations, and can be reflected by the overall Fe isotope fractionation between $Fe(II)_{aq}$ and $Fe(III)_{ppt}$. In this

study, isotope fractionation was evaluated quantitatively based on the assumption that Fe_{aq} represents residual Fe $(II)_{aq}$ while Fe_{ppt} represents the Fe(III) precipitates, which was reasonable based on Fe(II) and Fe(III) concentrations determined in Fe_{aq} and Fe_{ppt} (Fig. 1, Table 1). A Rayleigh fractionation model fits well to both the Fe_{aq} and Fe_{ppt} δ^{56}Fe data (Fig. 3, fitting line) which suggests that once Fe(III) precipitates form during enzymatic Fe(II) oxidation, they do not undergo isotopic exchange with the remaining aqueous Fe(II) within the time frame of these experiments. Rayleigh fitting of the δ^{56}Fe values for both Fe_{aq} and Fe_{ppt} of the three independent biological replicates resulted in a consistent uni-directional Fe isotopic fractionation $\varepsilon_{Fe(III)ppt\text{-}Fe(II)aq}$ of (2.0–2.4)‰ (Fig. 3).

Equilibrium isotope fractionation between $Fe(III)_{aq}$ and $Fe(II)_{aq}$ has experimentally been determined to be around 3‰ (Skulan et al., 2002; Welch et al., 2003; Balci et al., 2006). However, $Fe(III)_{aq}$ is not stable at the circumneutral pH conditions of our experiments, which results in rapid precipitation of Fe(III) minerals such as ferrihydrite, goethite, or lepidocrocite (Schwertmann et al., 1999). Importantly, the uni-directional precipitation of Fe(III) minerals imposes another Fe isotope fractionation, the extent of which depends on the reaction kinetics of precipitation (Skulan et al., 2002). This secondary Fe isotopic fractionation then influences the overall Fe isotope fractionation observed between $Fe(II)_{aq}$ and $Fe(III)_{ppt}$. The equilibrium isotopic fractionation ε^{56}Fe between ferrihydrite and $Fe(II)_{aq}$ was estimated to be around 3.2‰ (Wu et al., 2011), vs. 1.05‰ for goethite and $Fe(II)_{aq}$ (Beard et al., 2010), and 3.1‰ for hematite and $Fe(II)_{aq}$ (Wu et al., 2010). The Fe isotopic fractionation $\varepsilon_{Feppt\text{-}Feaq}$ of 2.3 ± 0.3‰ (2SD, $N = 6$) determined during phototrophic Fe(II) oxidation in the presence of Si is in between that of abiotically produced goethite and ferrihydrite/hematite. Yet our μXRD analysis (which had a detection limit of ~10% wt) did not detect any goethite or hematite in the Fe(III) precipitates (Fig. 2), which likely rules out the possibility of a mixture of goethite with hematite precipitation for producing an intermediate isotope fractionation ε^{56}Fe value of 2.3‰.

A comparison of our data to the Fe isotope fractionation values for phototrophic Fe(II) oxidation by the same bacterial strain in the absence of Si (Swanner et al., 2015) reveals some insights into the possible effect of Si on the isotopic exchange processes. In the absence of Si, distinct isotopic fractionation between Fe_{ppt} and Fe_{aq} was noted from Rayleigh fitting, with $\varepsilon^{56}Fe_{ppt\text{-}aq}$ values of 0.96–1.18‰ obtained from fitting $\delta^{56}Fe_{aq}$ datapoints, and 1.96–1.98‰ obtained from fitting the $\delta^{56}Fe_{ppt}$ data (Swanner et al., 2015). The unique fractionation for each Fe phase was attributed to processes such as $Fe(III)_{aq}$ complexation and colloid formation, which controlled the overall isotope fractionation between $Fe(II)_{aq}$ and $Fe(III)_{ppt}$ (Swanner et al., 2015). We now found that in the presence of Si, the fractionation factor calculated individually from both Fe_{aq} and Fe_{ppt} isotope data of our three experiments resulted in a very consistent Fe isotopic fractionation $\varepsilon_{Feppt\text{-}Feaq}$ value of 2.3 ± 0.3‰ (2SD, $N = 6$). This suggests that the Si has a strong controlling effect on the overall isotope fractionation of Fe between $Fe(II)_{aq}$ and $Fe(III)_{ppt}$, likely by controlling the formation of intermediate Fe species. Therefore, below we conducted an isotope composition calculation on the intermediate phases formed during Fe(II) oxidation, which may shed some light on the mechanism of how Si affects Fe isotope fractionation.

4.3. Calculated isotope compositions for intermediate Fe species

Concentration determinations for both Fe(II) and Fe (III) in the two extracted phases (Fe_{H2O} and Fe_{NaAc}) and Fe isotope measurements on the bulk H_2O and NaAc extracts enabled us to do mass balance calculations of the isotopic composition for sorbed or loosely bound Fe in our experiments. For this calculation we assumed that the Fe(II) in Fe_{H2O} had the same isotopic composition as the Fe(II) in Fe_{NaAc}, which we defined as $Fe(II)_{interm}$, and that the Fe(III) in Fe_{NaAc} and Fe_{H2O} had the same isotopic composition, which we defined as $Fe(III)_{interm}$, similar to a previous study (Crosby et al., 2007). The calculated isotopic compositions are shown in Table 2 and Fig. 3. Our calculations showed that, within the uncertainty range, most of the δ^{56}Fe values for $Fe(III)_{interm}$ were nearly the same as the Fe $(III)_{ppt}$, which indicates no significant net fractionation between $Fe(III)_{interm}$ and $Fe(III)_{ppt}$ during Fe mineral precipitation. The fractionation value resembles the estimated zero fractionation between $Fe(III)_{aq}$ and hematite at ambient temperature (Skulan et al., 2002).

Determination of the isotope fractionation values between $Fe(III)_{aq}$ and $Fe(III)_{ppt}$ is difficult due to the fast and complete precipitation (Skulan et al., 2002). At high temperature (98 °C), equilibrium isotope fractionation between $Fe(III)_{aq}$ and hematite was experimentally determined to be −0.1‰ (Skulan et al., 2002). Here in our study, poorly crystalline nanoparticle ferrihydrite likely formed, similar as observed in previous studies (Kappler and Newman, 2004). Equilibrium isotopic fractionation is ultimately determined by the bonding environment (Schauble, 2004). Given the structural similarity of ferrihydrite and hematite implicated by spectroscopic data, since hematite is a dehydrated form of ferrihydrite, and both have short Fe–Fe parings and face-sharing Fe octahedra (Schwertmann and Cornell, 2008), similar isotope fractionation between $Fe(III)_{aq}$ and ferrihydrite or hematite would be reasonable. Indeed, similar isotope fractionation for ferrihydrite and hematite with $Fe(II)_{aq}$ was also inferred in other studies (Wu et al., 2011). The near zero net fractionation between $Fe(III)_{interm}$ and $Fe(III)_{ppt}$, which resembles the value between $Fe(III)_{aq}$ and $Fe(III)_{ppt}$, suggests either an equilibrium isotope fractionation between $Fe(III)_{aq}$ and $Fe(III)_{interm}$ or that they do not exchange at all.

The calculated isotope composition for $Fe(II)_{interm}$ was always heavier than the δ^{56}Fe values of $Fe(II)_{aq}$ but lighter than $Fe(III)_{interm}$ or $Fe(III)_{ppt}$ (Fig. 3). The differences in δ^{56}Fe between $Fe(II)_{aq}$ and $Fe(II)_{interm}$ ranged from −1.2‰ to −0.4‰. This difference is likely caused by distinct isotopic fractionations during Fe(II) adsorption to Fe $(III)_{ppt}$. Adsorption of Fe(II) to Fe(III) minerals is known

to result in heavier $Fe(II)_{sorb}$ compared to non-sorbed, free $Fe(II)_{aq}$ (Icopini et al., 2004; Crosby et al., 2007). In particular, this difference was comparable to the experimentally determined average values of $-0.38 \pm 0.10‰$ and $-0.86 \pm 0.17‰$ between $Fe(II)_{aq}$ and $Fe(II)_{sorb}$ during bacterial Fe(III) reduction of hematite and goethite, individually (Crosby et al., 2005).

4.4. Si effect on Fe isotopic exchange

The extent of isotope fractionation during Fe redox transformation is a function of the reaction pathway and of the rates of redox transformation (Johnson et al., 2005). In particular sorption is an important process for isotopic exchange between aqueous Fe(II) and Fe minerals (Crosby et al., 2007; Handler et al., 2009). It was shown before that Si affects the Fe isotope fractionation between $Fe(II)_{aq}$ and Fe(III)-Si precipitates during dissimilatory Fe (III) reduction (Wu et al., 2009; Percak-Dennett et al., 2011) likely by changing the bonding environment of Fe (II) to Fe(III) minerals (Wu et al., 2009). Here we show that the presence of Si exerts some control on the isotopic exchange between the different Fe species during phototrophic Fe(II) oxidation. In the presence of Si, less intermediate Fe(II) was extracted from Fe_{ppt} in the $Fe(II)_{H2O}$ and $Fe(II)_{NaAc}$ fractions during phototrophic Fe(II) oxidation, suggesting less Fe(II) sorbs in the presence of Si, likely due to competition with Si for surface sites. Consequently the direct isotopic exchange between $Fe(II)_{aq}$ and $Fe(III)_{ppt}$ is prevented or at least minimized (Jones et al., 2009).

The effects of Si on Fe isotope fractionation showed a strong dependence on the Fe/Si ratio (Wu et al., 2012). This was attributed to the influence of Si on Fe(III) mineral precipitation (Doelsch et al., 2000; Pokrovski et al., 2003; Jones et al., 2009). In an abiotic Fe(II) oxidation experiment, the Fe isotope fractionation increased with increasing Si at a Fe/Si ratio of <1, while this trend was opposite at Fe/Si > 1 (Wu et al., 2012). This was attributed to the different crystal growth properties of Fe(III) minerals, i.e. at Fe/Si > 1, 3-D growth of Fe minerals with both edge and corner Fe–Fe linkages dominated, while at Fe/Si < 1, 2-D crystal growth with edge linkages dominated, and minimum Fe polymerization occurred at Fe/Si = 1 (Doelsch et al., 2000, 2003). During microbial Fe(II) oxidation, Si also affected Fe(III) precipitation, likely through Si substitution in Fe minerals, which resulted in crystal asymmetry and decreased crystallinity for the Fe minerals formed during phototrophic Fe(II) oxidation (Eickhoff et al., 2014; Gauger et al., 2016). The Fe isotopic fractionation determined between $Fe(III)_{ppt}$ and $Fe(II)_{aq}$ during phototrophic Fe(II) oxidation at 1.2 mM initial Fe(II) and 1 mM Si ($\varepsilon^{56}Fe_{ppt\text{-}aq} = 2.3 \pm 0.3‰$) is consistent with that determined between Si-ferrihydrite and Fe(II) at Fe/Si = 1 in abiotic setups ($2.58 \pm 0.14‰$) (Wu et al., 2011).

To determine what processes control fractionation during Fe(II) oxidation by *R. iodosum*, it is helpful to consider the two fundamental processes involved, which are $Fe(II)_{aq}$ oxidation to $Fe(III)_{aq}$ and $Fe(III)_{aq}$ precipitation as $Fe(III)_{ppt}$. As the calculated isotope compositions of $Fe(III)_{interm}$ suggest nearly no net fractionation among $Fe(III)_{aq}$, $Fe(III)_{interm}$ and $Fe(III)_{ppt}$, the second process likely had a minor contribution to the overall fractionation between $Fe(II)_{aq}$ and $Fe(III)_{ppt}$. In other words, the fractionation value ($\varepsilon^{56}Fe_{ppt\text{-}aq} = 2.3 \pm 0.3‰$) that differs from the well-studied equilibrium isotopic fractionation of around 3‰, is more likely due to the Fe(II) oxidation process where $Fe(II)_{aq}$ was oxidized to $Fe(III)_{aq}$ in the presence of Si. This is expected to be the case given that Fe isotope equilibrium fractionation between $Fe(II)_{aq}$ and $Fe(III)_{ppt}$ varies with the Fe/Si ratio (Wu et al., 2012). A sketch of the possible Fe isotope fractionation process during phototrophic Fe(II) oxidation by *R. iodosum* in the presence of Si is shown in Fig. 4 based on this hypothesis.

4.5. Geological implications

The observed effect of dissolved Si on Fe isotope fractionation during phototrophic Fe(II) oxidation has implications for Fe-containing aqueous environments where Si is or was present, in particular for ancient oceans. The Precambrian oceans were enriched in dissolved Si due to lack of efficient Si-utilization by higher organisms that were absent in the oceans until the Ediacaran age (Brasier et al., 1997). The concentration of dissolved Si in the Precambrian was estimated to be at saturation with cristobalite or amorphous Si in the range of 0.67–2.2 mM (Maliva et al., 2005), which was much higher than the average value in modern oceans (<0.10 mM) (Treguer et al., 1995), although Si concentrations up to 4 mM have also been reported in some modern natural waters (Pokrovski et al., 2003). Photoferrotrophs were suggested to be one of the most likely contributors for Fe(II) oxidation under anoxic or microoxic conditions in an early ocean (Kappler et al., 2005; Konhauser et al., 2007), and Si was likely incorporated in the precursor phase of Fe minerals before deposited in IFs such as iron silicates (Rasmussen et al., 2013, 2015) or Si-ferrihydrite precursors (Alibert and Kinsley, 2016). In the present study we observed a strong effect of Si on Fe species formation and on Fe isotopic exchange during microbial phototrophic Fe(II) oxidation at simulated Precambrian ferruginous and siliceous ocean conditions.

The fractionation factor $\varepsilon^{56}Fe_{ppt\text{-}aq} = 2.3 \pm 0.3‰$ between $\delta^{56}Fe(III)_{ppt}$ and $\delta^{56}Fe(II)_{aq}$ determined here has implications for the Fe isotope compositions in IFs precipitated throughout geological time. The hydrothermal source of Fe for IFs likely also contained Si. Therefore, co-precipitation of Si with Fe(III) oxyhydroxides, and the effect on the resulting Fe isotope composition of residual and precipitated Fe pools, needs to be considered. For example, Moeller et al. (2014) reported $\delta^{56}Fe$ values for modern microbial siliceous Fe-oxyhydroxide mounds from the Jan Mayen vent fields, Norwegian-Greenland Sea, between −2.09‰ and −0.66‰, which, with one exception, are equal or isotopically heavier than the low-temperature hydrothermal fluids with $\delta^{56}Fe$ values of −1.84‰ and −1.53‰ from which these Fe deposits formed. Similarly, $\delta^{56}Fe$ values between −0.38‰ and 0.89‰ for microbial jaspilitic plume deposits from the Ordovician Løkken ophiolite complex, W-Norway reported in the same study are equal or isotopically heavier than modern high-

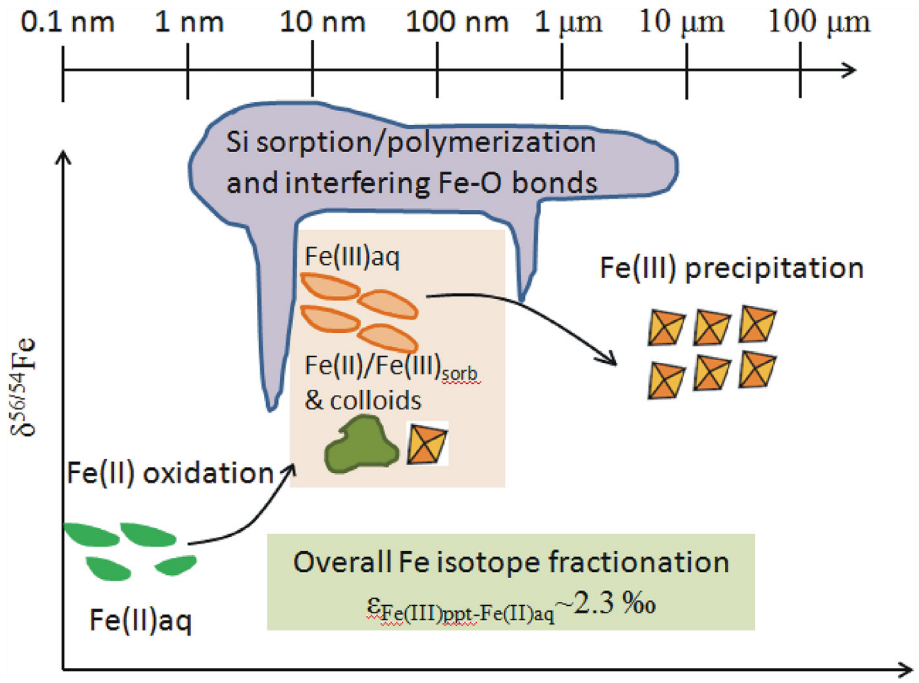

Fig. 4. A sketch of Fe isotope fractionation processes during phototrophic Fe(II) oxidation in the presence of Si. At least two processes were involved: $Fe(II)_{aq}$ oxidation and $Fe(III)_{aq}$ precipitation. Fewer intermediate phases of Fe_{H2O} and Fe_{NaAc} (i.e. sorbed, colloidal, or organically complexed Fe(II) or Fe(III)) formed in the presence of Si, which prevents Fe isotope exchange, likely by sorption, complexation, and co-precipitation, resulting in an overall isotope fraction $\varepsilon^{56}Fe_{ppt\text{-}aq}$ of $2.3 \pm 0.3‰$ between Fe precipitates and $Fe(II)_{aq}$.

temperature vent fluids with $\delta^{56}Fe$ values of ca. −0.8‰ to −0.2‰ (Sharma et al., 2001; Beard et al., 2003b; Severmann et al., 2004; Rouxel et al., 2008; Bennett et al., 2009) The proposed interpretation of these data by partial microbial $Fe(II)_{aq}$ oxidation in a Si-bearing environment and subsequent deposition in mounds with no or little post-depositional Fe cycling by Fe(III)-reducing bacteria through dissimilatory iron reduction (DIR) (Moeller et al., 2014) agrees well with the results of this study. Our fractionation factor $\varepsilon^{56}Fe_{ppt\text{-}aq} = 2.3 \pm 0.3‰$ between $\delta^{56}Fe(III)_{ppt}$ and $\delta^{56}Fe(II)_{aq}$, if applicable to modern low-temperature siliceous microbial Fe-hydroxide deposits and ancient high/medium-temperature microbial jaspilitic plume deposits, might then be used to calculate the proportion of partial microbial $Fe(II)_{aq}$ oxidation in siliceous environments, as was done by Moeller et al. (2014) using somewhat higher fractionation factors $\varepsilon^{56}Fe_{ppt\text{-}aq}$ of 2.58–3.99‰ between $\delta^{56}Fe(III)_{ppt}$ and $\delta^{56}Fe(II)_{aq}$, reported by Wu et al. (2011, 2012) for abiotic (Si-free and Si-bearing) systems. Moreover, Fe isotope exchange between different Fe fractions is prevented when Fe minerals are precipitated in the presence of Si, as we show in our work and has been suggested by others (Doelsch et al., 2003; Pokrovski et al., 2003; Jones et al., 2009; Wu et al., 2012). Aside from influencing Fe isotope compositions of residual and precipitated Fe pools, the presence of Si, regardless of the Fe(II) oxidation pathway (i.e. biotic or abiotic), may even reduce the mobility of trace elements (e.g. Ni) that are co-precipitated with Fe minerals (Frierdich et al., 2011), by blocking the reaction sites of Fe mineral recrystallization that was shown to lead to a mobilization of trace metals. As Precambrian IFs Ni concentrations have been suggested to reflect the composition of trace elements in seawater during formation, and thus control the activity of microbes dependent on those elements (Konhauser et al., 2009, 2015), the presence of Si during precipitation may support the fidelity of IFs trace element archives.

5. CONCLUSIONS

Fe isotope fractionation during phototrophic Fe(II) oxidation in the presence of Si was clearly different from that in the absence of Si, i.e. with Si the fractionation factors generated individually from $Fe(II)_{aq}$ and $Fe(III)_{ppt}$ were consistent (Table 2 and Fig. 3) while they differed in setups without Si (Swanner et al., 2015). This clearly suggests a role of Si in minimizing isotopic exchange processes between different Fe species during phototrophic Fe(II) oxidation. As a consequence, the presence of Si would likely have affected the Fe speciation and Fe isotopic composition of the Fe precipitates and this has to be considered when analyzing Fe isotope composition values for different Fe-containing minerals in Precambrian IFs.

ACKNOWLEDGEMENTS

We would like to thank Viktoria Soos and Markus Maisch for help with Fe speciation analysis, Maximilian Halama for μ-XRD measurements, and Kay Simmack for Fe purification. This study was supported by NSFC (No. 41502320), CSC-DAAD postdoc scholarship, China Postdoc Science Foundation (No. 2014M560115). Andreas Kappler was supported by the European Research Council (ERC), grant Agreement No. 307320-

MICROFOX. The Fe isotope measurements performed in the Isotope Geochemistry Laboratories of Ronny Schoenberg were funded by DFG grant KA 1736/27-1.

REFERENCES

Alibert C. and Kinsley L. (2016) Ge/Si in Hamersley BIF as tracer of hydrothermal Si and Ge inputs to the Paleoproterozoic ocean. *Geochim. Cosmochim. Acta* **184**, 329–343.

Alleon J., Bernard S., Le Guillou C., Marin-Carbonne J., Pont S., Beyssac O., McKeegan K. D. and Robert F. (2016) Molecular preservation of 1.88 Ga Gunflint organic microfossils as a function of temperature and mineralogy. *Nat. Commun.* **7**. http://dx.doi.org/10.1038/ncomms11977.

Anbar A. D. and Knoll A. H. (2002) Proterozoic ocean chemistry and evolution: a bioinorganic bridge? *Science* **297**, 1137–1142.

Anbar A. D., Roe J. E., Barling J. and Nealson K. H. (2000) Nonbiological fractionation of iron isotopes. *Science* **288**, 126–128.

Balci N., Bullen T. D., Witte-Lien K., Shanks W. C., Motelica M. and Mandernack K. W. (2006) Iron isotope fractionation during microbially stimulated Fe (II) oxidation and Fe (III) precipitation. *Geochim. Cosmochim. Acta* **70**, 622–639.

Beard B., Handler R., Scherer M., Wu L., Czaja A., Heimann A. and Johnson C. (2010) Iron isotope fractionation between aqueous ferrous iron and goethite. *Earth Planet. Sci. Lett.* **295**, 241–250.

Beard B., Johnson C., Cox L., Sun H., Nealson K. and Aguilar C. (1999) Iron isotope biosignatures. *Science* **285**, 1889–1892.

Beard B. L., Johnson C. M., Skulan J. L., Nealson K. H., Cox L. and Sun H. (2003a) Application of Fe isotopes to tracing the geochemical and biological cycling of Fe. *Chem. Geol.* **195**, 87–117.

Beard B. L., Johnson C. M., Von Damm K. L. and Poulson R. L. (2003b) Iron isotope constraints on Fe cycling and mass balance in oxygenated Earth oceans. *Geology* **31**, 629–632.

Bennett S. A., Rouxel O., Schmidt K., Garbe-Schönberg D., Statham P. J. and German C. R. (2009) Iron isotope fractionation in a bouyant hydrothermal plume, 5°S Mid-Atlantic Ridge. *Geochim. Cosmochim. Acta* **73**, 5619–5634.

Bekker A., Slack J. F., Planavsky N., Krapez B., Hofmann A., Konhauser K. O. and Rouxel O. J. (2010) Iron formation: the sedimentary product of a complex interplay among mantle, tectonic, oceanic, and biospheric processes. *Econ. Geol.* **105**, 467–508.

Brasier M., Green O. and Shields G. (1997) Ediacarian sponge spicule clusters from southwestern Mongolia and the origins of the Cambrian fauna. *Geology* **25**, 303–306.

Chan C. S. and Emerson D. (2016) The role of microaerophilic Fe-oxidizing micro-organisms in producing banded iron formations. *Geobiology* **14**.

Chan C. S., Fakra S. C., Emerson D., Fleming E. J. and Edwards K. J. (2011) Lithotrophic iron-oxidizing bacteria produce organic stalks to control mineral growth: implications for biosignature formation. *ISME J.* **5**, 717–727.

Croal L., Jiao Y., Kappler A. and Newman D. (2009) Phototrophic Fe(II) oxidation in an atmosphere of H_2: implications for Archean banded iron formations. *Geobiology* **7**, 21–24.

Croal L., Johnson C., Beard B. and Newman D. (2004) Iron isotope fractionation by Fe (II)-oxidizing photoautotrophic bacteria. *Geochim. Cosmochim. Acta* **68**, 1227–1242.

Crosby C. H., Bailey J. V. and Sharma M. (2014) Fossil evidence of iron-oxidizing chemolithotrophy linked to phosphogenesis in the wake of the Great Oxidation Event. *Geology* **42**, 1015–1018.

Crosby H., Johnson C., Roden E. and Beard B. (2005) Coupled Fe (II)-Fe(III) electron and atom exchange as a mechanism for Fe isotope fractionation during dissimilatory iron oxide reduction. *Environ. Sci. Technol.* **39**, 6698–6704.

Crosby H. A., Roden E. E., Johnson C. M. and Beard B. L. (2007) The mechanisms of iron isotope fractionation produced during dissimilatory Fe (III) reduction by *Shewanella putrefaciens* and *Geobacter sulfurreducens*. *Geobiology* **5**, 169–189.

Crowe S. A., Dossing L. N., Beukes N. J., Bau M., Kruger S. J., Frei R. and Canfield D. E. (2013) Atmospheric oxygenation three billion years ago. *Nature* **501**, 535–538.

Czaja A. D., Johnson C. M., Beard B. L., Eigenbrode J. L., Freeman K. H. and Yamaguchi K. E. (2010) Iron and carbon isotope evidence for ecosystem and environmental diversity in the ~2.7 to 2.5 Ga Hamersley Province, Western Australia. *Earth Planet. Sci. Lett.* **292**, 170–180.

Czaja A. D., Johnson C. M., Beard B. L., Roden E. E., Li W. and Moorbath S. (2013) Biological Fe oxidation controlled deposition of banded iron formation in the ca. 3770 Ma Isua Supracrustal Belt (West Greenland). *Earth Planet. Sci. Lett.* **363**, 192–203.

Delstanche S., Opfergelt S., Cardinal D., Elsass F., André L. and Delvaux B. (2009) Silicon isotopic fractionation during adsorption of aqueous monosilicic acid onto iron oxide. *Geochim. Cosmochim. Acta* **73**, 923–934.

Doelsch E., Masion A., Rose J., Stone W., Bottero J. and Bertsch P. (2003) Chemistry and structure of colloids obtained by hydrolysis of Fe (III) in the presence of SiO_4 ligands. *Colloids Surf. A* **217**, 121–128.

Doelsch E., Rose J., Masion A., Bottero J. Y., Nahon D. and Bertsch P. M. (2000) Speciation and crystal chemistry of iron (III) chloride hydrolyzed in the presence of SiO_4 ligands. 1 An Fe K-edge EXAFS study. *Langmuir* **16**, 4726–4731.

Doelsch E., Stone W. E., Petit S., Masion A., Rose J., Bottero J.-Y. and Nahon D. (2001) Speciation and crystal chemistry of Fe (III) chloride hydrolyzed in the presence of SiO_4 ligands. 2. Characterization of Si-Fe aggregates by FTIR and ^{29}Si solid-state NMR. *Langmuir* **17**, 1399–1405.

Dodd M. S., Papineau D., Grenne T., Slack J. F., Rittner M., Pirajno F., O'Neil J. and Little C. T. S. (2017) Evidence for early life in Earth's oldest hydrothermal vent precipitates. *Nature* **543**, 60–64.

Ehrenreich A. and Widdel F. (1994) Anaerobic oxidation of ferrous iron by purple bacteria, a new type of phototrophic metabolism. *Appl. Environ. Microbiol.* **60**, 4517–4526.

Eickhoff M., Birgel D., Talbot H., Peckmann J. and Kappler A. (2013) Oxidation of Fe (II) leads to increased C-2 methylation of pentacyclic triterpenoids in the anoxygenic phototrophic bacterium *Rhodopseudomonas palustris* strain TIE-1. *Geobiology* **11**. http://dx.doi.org/10.1111/gbi.12033.

Eickhoff M., Obst M., Schröder C., Hitchcock A. P., Tyliszczak T., Martinez R. E., Robbins L. J., Konhauser K. O. and Kappler A. (2014) Nickel partitioning in biogenic and abiogenic ferrihydrite: the influence of silica and implications for ancient environments. *Geochim. Cosmochim. Acta* **140**, 65–79.

Frierdich A. J., Luo Y. and Catalano J. G. (2011) Trace element cycling through iron oxide minerals during redox-driven dynamic recrystallization. *Geology* **39**(11), 1083–1086.

Fru E. C., Ivarsson M., Kilias S. P., Bengtson S., Belivanova V., Marone F., Fortin D., Broman C. and Stampanoni M. (2013) Fossilized iron bacteria reveal a pathway to the biological origin of banded iron formation. *Nat. Commun.* **4**. http://dx.doi.org/10.1038/ncomms3050.

Gauger T., Byrne J. M., Konhauser K. O., Obst M., Crowe S. and Kappler A. (2016) Influence of organics and silica on Fe(II) oxidation rates and cell–mineral aggregate formation by the

green-sulfur Fe(II)-oxidizing bacterium *Chlorobium ferrooxidans* KoFox – implications for Fe(II) oxidation in ancient oceans. *Earth Planet. Sci. Lett.* **443**, 81–89.

Gauger T., Konhauser K. and Kappler A. (2015) Protection of phototrophic iron (II)-oxidizing bacteria from UV irradiation by biogenic iron (III) minerals: implications for early Archean banded iron formation. *Geology* **43**, 1067–1070.

Handler R. M., Beard B. L., Johnson C. M. and Scherer M. M. (2009) Atom exchange between aqueous Fe (II) and goethite: an Fe isotope tracer study. *Environ. Sci. Technol.* **43**, 1102–1107.

Hashizume K., Pinti D., Orberger B., Cloquet C., Jayananda M. and Soyama H. (2016) A biological switch at the ocean surface as a cause of laminations in a Precambrian iron formation. *Earth Planet. Sci. Lett.* **446**, 27–36.

Hegler F., Posth N., Jiang J. and Kappler A. (2008) Physiology of phototrophic iron (II)-oxidizing bacteria: implications for modern and ancient environments. *FEMS Microbiol. Ecol.* **66**, 250–260.

Heimann A., Johnson C. M., Beard B. L., Valley J. W., Roden E. E., Spicuzza M. J. and Beukes N. J. (2010) Fe, C, and O isotope compositions of banded iron formation carbonates demonstrate a major role for dissimilatory iron reduction in ~2.5 Ga marine environments. *Earth Planet. Sci. Lett.* **294**, 8–18.

Hill P. S., Schauble E. A. and Young E. D. (2010) Effects of changing solution chemistry on Fe^{3+}/Fe^{2+} isotope fractionation in aqueous Fe–Cl solutions. *Geochim. Cosmochim. Acta* **74**, 6669–6689.

Hohmann C., Winkler E., Morin G. and Kappler A. (2009) Anaerobic Fe(II)-oxidizing bacteria show as resistance and immobilize as during Fe(III) mineral precipitation. *Environ. Sci. Technol.* **44**, 94–101.

Holland H. D. (2002) Volcanic gases, black smokers, and the Great Oxidation Event. *Geochim. Cosmochim. Acta* **66**, 3811–3826.

Icopini G., Anbar A., Ruebush S., Tien M. and Brantley S. (2004) Iron isotope fractionation during microbial reduction of iron: the importance of adsorption. *Geology* **32**, 205.

Johnson C. M. and Beard B. L. (2005) Biogeochemical cycling of iron isotopes. *Science* **309**, 1025–1027.

Johnson C. M., Beard B. L., Beukes N. J., Klein C. and O'Leary J. M. (2003) Ancient geochemical cycling in the Earth as inferred from Fe isotope studies of banded iron formations from the Transvaal Craton. *Contrib. Miner. Petrol.* **144**, 523–547.

Johnson C. M., Beard B. L., Klein C., Beukes N. J. and Roden E. E. (2008a) Iron isotopes constrain biologic and abiologic processes in banded iron formation genesis. *Geochim. Cosmochim. Acta* **72**, 151–169.

Johnson C. M., Beard B. L. and Roden E. E. (2008b) The iron isotope fingerprints of redox and biogeochemical cycling in modern and ancient Earth. *Annu. Rev. Earth Planet. Sci.* **36**, 457–493.

Johnson C. M., Roden E. E., Welch S. A. and Beard B. L. (2005) Experimental constraints on Fe isotope fractionation during magnetite and Fe carbonate formation coupled to dissimilatory hydrous ferric oxide reduction. *Geochim. Cosmochim. Acta* **69**, 963–993.

Jones A. M., Collins R. N., Rose J. and Waite T. D. (2009) The effect of silica and natural organic matter on the Fe (II)-catalysed transformation and reactivity of Fe(III) minerals. *Geochim. Cosmochim. Acta* **73**, 4409–4422.

Kappler A., Johnson C., Crosby H., Beard B. and Newman D. (2010) Evidence for equilibrium iron isotope fractionation by nitrate-reducing iron(II)-oxidizing bacteria. *Geochim. Cosmochim. Acta* **74**, 2826–2842.

Kappler A. and Newman D. K. (2004) Formation of Fe(III)-minerals by Fe(II)-oxidizing photoautotrophic bacteria. *Geochim. Cosmochim. Acta* **68**, 1217–1226.

Kappler A., Pasquero C., Konhauser K. O. and Newman D. K. (2005) Deposition of banded iron formations by anoxygenic phototrophic Fe(II)-oxidizing bacteria. *Geology* **33**, 865–868.

Konhauser K. O., Amskold L., Lalonde S. V., Posth N. R., Kappler A. and Anbar A. (2007) Decoupling photochemical Fe (II) oxidation from shallow-water BIF deposition. *Earth Planet. Sci. Lett.* **258**, 87–100.

Konhauser K. O., Hamade T., Raiswell R., Morris R. C., Ferris F. G., Southam G. and Canfield D. E. (2002) Could bacteria have formed the Precambrian banded iron formations? *Geology* **30**, 1079–1082.

Konhauser K. O., Pecoits E., Lalonde S. V., Papineau D., Nisbet E. G., Barley M. E., Arndt N. T., Zahnle K. and Kamber B. S. (2009) Oceanic nickel depletion and a methanogen famine before the Great Oxidation Event. *Nature* **458**, 750–754.

Konhauser K. O., Robbins L. J., Pecoits E., Peacock C., Kappler A. and Lalonde S. V. (2015) The Archean nickel famine revisited. *Astrobiology* **15**, 804–815.

Luo G., Ono S., Beukes N. J., Wang D. T., Xie S. and Summons R. E. (2016) Rapid oxygenation of Earth's atmosphere 2.33 billion years ago. *Sci. Adv.* **2**, e1600134.

Maliva R. G., Knoll A. H. and Simonson B. M. (2005) Secular change in the Precambrian silica cycle: insights from chert petrology. *Geol. Soc. Am. Bull.* **117**, 835–845.

Moeller K., Schoenberg R., Grenne T., Thorseth I. H., Drost K. and Pedersen R. B. (2014) Comparison of iron isotope variations in modern and Ordovician siliceous Fe oxyhydroxide deposits. *Geochim. Cosmochim. Acta* **126**, 422–440.

Percak-Dennett E. M., Beard B. L., Xu H., Konishi H., Johnson C. M. and Roden E. E. (2011) Iron isotope fractionation during microbial dissimilatory iron oxide reduction in simulated Archaean seawater. *Geobiology* **9**, 205–220.

Picard A., Kappler A., Schmid G., Quaroni L. and Obst M. (2015) Experimental diagenesis of organo-mineral structures formed by microaerophilic Fe (II)-oxidizing bacteria. *Nat. Commun.* **6**. http://dx.doi.org/10.1038/ncomms7277.

Planavsky N., Rouxel O. J., Bekker A., Hoffman A., Little C. T. and Lyons T. W. (2012) Iron isotope composition of some Archean and Proterozoic iron formations. *Geochim. Cosmochim. Acta* **80**, 158–169.

Planavsky N. J., Dan A., Hofmann A., Reinhard C. T., Lalonde S. V., Knudsen A., Wang X., Ossa F. O., Pecoits E. and Smith A. J. B. (2014) Evidence for oxygenic photosynthesis half a billion years before the Great Oxidation Event. *Nat. Geosci.* **7**, 283–286.

Pokrovski G. S., Schott J., Farges F. and Hazemann J.-L. (2003) Iron (III)-silica interactions in aqueous solution: insights from X-ray absorption fine structure spectroscopy. *Geochim. Cosmochim. Acta* **67**, 3559–3573.

Posth N., Canfield D. and Kappler A. (2014) Biogenic Fe (III) minerals: from formation to diagenesis and preservation in the rock record. *Earth Sci. Rev.* **135**, 103–121.

Posth N. R., Hegler F., Konhauser K. O. and Kappler A. (2008) Alternating Si and Fe deposition caused by temperature fluctuations in Precambrian oceans. *Nat. Geosci.* **1**, 703–708.

Rasmussen B., Krapež B., Muhling J. R. and Suvorova A. (2015) Precipitation of iron silicate nanoparticles in early Precambrian oceans marks Earth's first iron age. *Geology* **43**, 303–306.

Rasmussen B., Meier D. B., Krapež B. and Muhling J. R. (2013) Iron silicate microgranules as precursor sediments to 2.5-billion-year-old banded iron formations. *Geology* **41**, 435–438.

Reddy T. R., Zheng X.-Y., Roden E. E., Beard B. L. and Johnson C. M. (2016) Silicon isotope fractionation during microbial reduction of Fe (III)–Si gels under Archean seawater conditions and implications for iron formation genesis. *Geochim. Cosmochim. Acta* **190**, 85–99.

Rouxel O. J., Bekker A. and Edwards K. J. (2005) Iron isotope constraints on the Archean and Paleoproterozoic ocean redox state. *Science* **307**, 1088–1091.

Rouxel O., Shanks, III, W. C., Bach W. and Edwards K. J. (2008) Integrated Fe- and S-isotope study of seafloor hydrothermal vents at East Pacific Rise 9–10°N. *Chem. Geol.* **252**, 214–227.

Schauble E. A. (2004) Applying stable isotope fractionation theory to new systems. *Rev. Mineral. Geochem.* **55**, 65–111.

Schoenberg R. and von Blanckenburg F. (2005) An assessment of the accuracy of stable Fe isotope ratio measurements on samples with organic and inorganic matrices by high-resolution multicollector ICP-MS. *Int. J. Mass Spectrom.* **242**, 257–272.

Schwertmann U. and Cornell R. M. (2008) *Iron Oxides in the Laboratory*. John Wiley & Sons.

Schwertmann U., Friedl J. and Stanjek H. (1999) From Fe(III) ions to ferrihydrite and then to hematite. *J. Colloid Interface Sci.* **209**, 215–223.

Severmann S., Johnson C. M., Beard B. L., German C. R., Edmonds H. N., Chiba H. and Green D. R. H. (2004) The effect of plume processes on the Fe isotope composition of hydrothermally derived Fe in the deep ocean as inferred from the Rainbow vent site, Mid-Atlantic Ridge, 36°14′N. *Earth Planet. Sci. Lett.* **225**, 63–76.

Sharma M., Polizzotto M. and Anbar A. D. (2001) Iron isotopes in hot springs along the Juan de Fuca Ridge. *Earth Planet. Sci. Lett.* **194**, 39–51.

Skulan J. L., Beard B. L. and Johnson C. M. (2002) Kinetic and equilibrium Fe isotope fractionation between aqueous Fe (III) and hematite. *Geochim. Cosmochim. Acta* **66**, 2995–3015.

Stookey L. (1970) Ferrozine – a new spectrophotometric reagent for iron. *Anal. Chem.* **42**, 779–781.

Straub K. L., Rainey F. A. and Widdel F. (1999) *Rhodovulum iodosum* sp. nov. and *Rhodovulum robiginosum* sp. nov., two new marine phototrophic ferrous-iron-oxidizing purple bacteria. *Int. J. Syst. Bacteriol.* **49**, 729–735.

Strickland J. D. H. and Parsons T. R. (1972) *A Practical Handbook of Seawater Analysis*. Fisheries Research Board of Canada, p. 167.

Swanner E. D., Wu W., Schoenberg R., Byrne J., Michel F. M., Pan Y. and Kappler A. (2015) Fractionation of Fe isotopes during Fe(II) oxidation by a marine photoferrotroph is controlled by the formation of organic Fe-complexes and colloidal Fe fractions. *Geochim. Cosmochim. Acta* **165**, 44–61.

Tosca N. J., Guggenheim S. and Pufahl P. K. (2016) An authigenic origin for Precambrian greenalite: implications for iron formation and the chemistry of ancient seawater. *Geol. Soc. Am. Bull.* **128**, 511–530.

Treguer P., Nelson D. M., Van Bennekom A. J. and DeMaster D. J. (1995) The silica balance in the world ocean: a reestimate. *Science* **268**, 375.

Welch S., Beard B., Johnson C. and Braterman P. (2003) Kinetic and equilibrium Fe isotope fractionation between aqueous Fe (II) and Fe (III). *Geochim. Cosmochim. Acta* **67**, 4231–4250.

Wu L., Beard B. L., Roden E. E. and Johnson C. M. (2009) Influence of pH and dissolved Si on Fe isotope fractionation during dissimilatory microbial reduction of hematite. *Geochim. Cosmochim. Acta* **73**, 5584–5599.

Wu L., Beard B. L., Roden E. E. and Johnson C. M. (2011) Stable iron isotope fractionation between aqueous Fe(II) and hydrous ferric oxide. *Environ. Sci. Technol.* **45**, 1847–1852.

Wu L., Beard B. L., Roden E. E., Kennedy C. B. and Johnson C. M. (2010) Stable Fe isotope fractionations produced by aqueous Fe(II)-hematite surface interactions. *Geochim. Cosmochim. Acta* **74**, 4249–4265.

Wu L., Percak-Dennett E. M., Beard B. L., Roden E. E. and Johnson C. M. (2012) Stable iron isotope fractionation between aqueous Fe(II) and model Archean ocean Fe–Si coprecipitates and implications for iron isotope variations in the ancient rock record. *Geochim. Cosmochim. Acta* **84**, 14–28.

Wu W., Swanner E. D., Hao L., Zeitvogel F., Obst M., Pan Y. and Kappler A. (2014) Characterization of the physiology and cell–mineral interactions of the marine anoxygenic phototrophic Fe (II) oxidizer *Rhodovulum iodosum* – implications for Precambrian Fe (II) oxidation. *FEMS Microbiol. Ecol.* **88**, 503–515.

Zheng X.-Y., Beard B. L., Reddy T. R., Roden E. E. and Johnson C. M. (2016) Abiologic silicon isotope fractionation between aqueous Si and Fe(III)–Si gel in simulated Archean seawater: Implications for Si isotope records in Precambrian sedimentary rocks. *Geochim. Cosmochim. Acta.* **187**, 102–122.

Associate editor: Stefan Weyer